ON THE INTEGRALITY GAP OF SMALL ASYMMETRIC TRAVELING SALESMAN PROBLEMS: A POLYHEDRAL AND COMPUTATIONAL APPROACH

Eleonora Vercesi ✉, Luca Maria Gambardella
Faculty of Informatics,
Università della Svizzera italiana (USI)
Lugano, Switzerland {eleonora.vercesi,luca.gambardella}@usi.ch

Janos Barta, Monaldo Mastrolilli
Dipartimento Tecnologie innovative,
Scuola universitaria professionale della Svizzera italiana (SUPSI)
Lugano, Switzerland {janos.barta, monaldo.mastrolilli}@supsi.ch

Stefano Gualandi
Department of Mathematics "Felice Casorati"
University of Pavia
Pavia, Italy
stefano.gualandi@unipv.it

ABSTRACT

In this paper, we investigate the integrality gap of the Asymmetric Traveling Salesman Problem (ATSP) with respect to the linear relaxation given by the Asymmetric Subtour Elimination Problem (ASEP) for instances with n nodes, where n is small. In particular, we focus on the geometric properties and symmetries of the ASEP polytope (P^n_{ASEP}) and its vertices. The polytope's symmetries are exploited to design a heuristic pivoting algorithm to search vertices where the integrality gap is maximized. Furthermore, a general procedure for the extension of vertices from P^n_{ASEP} to P^{n+1}_{ASEP} is defined. The generated vertices improve the known lower bounds of the integrality gap for $16 \leq n \leq 22$ and, provide small hard-to-solve ATSP instances.

***K*eywords** Asymmetric Traveling Salesman Problem · Integrality Gap

1 Introduction

The use of integer linear programming in modeling has been instrumental in both the practical solution of combinatorial optimization problems (See, e.g. [1]) and the formulation and analysis of approximation algorithms (See, e.g [31]). When solving an instance, an important concept is the *integrality gap* (IG) with respect to the linear relaxation, which is the maximum ratio between the solution quality of the Integer Linear Program (ILP) and its Linear Program (LP) relaxation. For many integer linear programs, the integrality gap of the linear relaxation is equal to the approximation ratio of the best algorithm, as well as the hardness of the approximation ratio, and essentially represents the inherent limits of the considered relaxation. To some extent, instances having a large integrality gap are the hard instances for the class of approaches based on linear programming. With this respect, the following facts can be observed from the literature.

- Proving integrality gaps for LP relaxations of NP-hard optimization problems is a difficult task that is usually undertaken on a case-by-case basis (e.g., see the case of the Vertex Cover [29]). Very few and limited attempts have been made to use computer-assisted analysis for this difficult goal.
- For several notable and important examples, like the Traveling Salesman Problem (TSP), our integrality gap comprehension has resisted the persistent attack during the last decades of many researchers. For the Symmetric Traveling Salesman Problem (STSP), several advances have been made in specific cases, such as the STSP having only costs 1 and 2 [25], and the cubic and subcubic STSP [6], where the integrality gap is proved to be equal to $\frac{4}{3}$. For the asymmetric case, [9, 13] exhibit two different families of ATSP instances of increasing size with an integrality gap asymptotically tending to 2. This, in turn, implies that the lower bound for the integrality gap is 2, and no further improvements have been made. More specifically, [13] also provides specific lower bounds for $n \leq 15$, where n is the number of nodes. This is the first time an IG greater than $\frac{4}{3}$ is shown for $n = 9$. In terms of the upper bound, the best-known bound is constant and equal to 22 [30].

Within this paper, we investigate the integrality gap *computationally* for the Asymmetric Traveling Salesman Problem. More specifically, we investigate and exploit aspects of polyhedral theory to reduce the integrality gap search space. Then, we combine this information to effectively search the pruned space. This approach allows us to get computer-aided construction of bad instances, namely, problem instances having large integrality gap values, for the considered LP relaxation, which improves upon the best-known lower bounds for small n (see Charikar, Goemans, and Karloff [9] and Elliot-Magwood [13]). The aim is to obtain a new and better understanding of lower bounds on the corresponding integrality gaps. As a side result, we present hard-to-solve ATSP instances.

The problem Given a weighted directed graph, a Hamiltonian cycle is a cycle that visits each node exactly once. The Asymmetric Traveling Salesman Problem (ATSP) involves finding a directed Hamiltonian cycle of minimum cost. In practice, the currently most efficient exact algorithm for solving ATSP is based on an Integer Linear Programming (ILP) formulation [14, 15, 28]. Let $K_n = (V, A)$ be the complete directed graph with n nodes and $m = n(n-1)$ arcs, that is, $V := \{1, \ldots, n\}$ and $A := \{(i,j) \mid i, j \in V, i \neq j\}$, each having a weight $c_{ij} \in \mathbb{R}^+$. Whenever $c_{ij} = c_{ji}$ for all arcs (i,j), then we have a Symmetric TSP instance. Whenever $c_{ij} \neq c_{ji}$, but the cost vector satisfies the triangle inequality $c_{ij} \leq c_{ik} + c_{kj}, \forall i, j, k \in V$, we have a pseudo-quasi metric TSP instance, since the cost vector induces a *pseudo-quasi metric* [24]. Note that any instance of ATSP on a complete graph K_n is completely defined by its cost vector $\boldsymbol{c} \in \mathbb{R}^m_+$. Given $S \subset V$, let $\delta(S)$ be the cut induced by S, namely $\delta(S) := \{(i,j) \mid i \in S, j \notin S\}$. For convenience, we denote $\delta(i) = \delta(\{i\})$.

In this paper, we study the LP relaxation of the Dantzig-Fulkerson-Johnson (DFJ) formulation [12] for solving the ATSP for small values of n.

$$\min \quad \sum_{(i,j) \in A} c_{ij} x_{ij} \tag{1}$$

$$\text{s.t.} \quad \sum_{i \in V} x_{ij} = 1 \qquad \forall j \in V \tag{2}$$

$$\sum_{j \in V} x_{ij} = 1 \qquad \forall i \in V \tag{3}$$

$$\sum_{(i,j) \in \delta(S)} x_{ij} \geq 1 \qquad \forall S \subset V \text{ such that } 2 \leq |S| \leq n-2 \tag{4}$$

$$x_{ij} \in \{0, 1\} \qquad \forall (i,j) \in A, \tag{5}$$

where $x_{ij} \in \{0,1\}$ is equal to 1 if arc (i,j) belongs to an optimal cycle, and 0 otherwise. Constraints (2)–(3) are the in-degree and out-degree constraints, which force each node to have exactly one predecessor and one successor. Constraints (4) are the *Subtour Elimination Constraints*, which avoid the presence of sub-cycles (subtours). For a survey on ATSP formulations, we refer the reader to [28]. In the literature, the solution of the LP relaxation of (1)–(5) is called the *Asymmetric Subtour Elimination Problem* (ASEP), while the corresponding feasibility region is the *ASEP Polytope*, which is defined as follows.

$$P^n_{ASEP} := \{\boldsymbol{x} \in \mathbb{R}^m \mid (2)\text{–}(4), \boldsymbol{x} \geq 0\}. \tag{6}$$

The Integrality Gap for the ATSP on n nodes is

$$\alpha_n := \sup_{c \in \mathbb{R}^m_+} \frac{\text{ATSP}(\boldsymbol{c})}{\text{ASEP}(\boldsymbol{c})}, \tag{7}$$

where ATSP($\boldsymbol{c}$) is the optimal value of (1)–(5) and ASEP($\boldsymbol{c}$) is the optimal value of its LP relaxation. In general, the IG for the ATSP is

$$\alpha := \sup_{n \in \mathbb{N}} \alpha_n.$$

In [13], it is shown that for the general ATSP, a non-negative cost vector $\boldsymbol{c}$ exists such that ATSP($\boldsymbol{c}$) > 0 and ASEP($\boldsymbol{c}$) $= 0$. This implies that the integrality gap tends to $+\infty$. For this reason, the works studying the integrality gap of ATSP always assume that the cost vector satisfies the triangle inequality $c_{ij} \leq c_{ik} + c_{kj}, \forall i, j, k \in V$ and, hence, the costs induce a pseudo-quasi metric. Herein, we restrict our attention to pseudo-quasi-metric ATSP, but we will call them ATSP for short, to be consistent with the notation of the literature.

A long-standing conjecture stated that $\alpha \leq \frac{4}{3}$ (e.g., see [8]). However, this conjecture was disproved in [9, 13], where it has been shown that $\alpha \geq 2$ by presenting two families of ATSP instances with $\alpha(\boldsymbol{c}) \to 2$ for $n \to \infty$. For $n \leq 3$, we have that $\alpha_n = 1$, while for $4 \leq n \leq 7$ the exact value was computed in [13]. The authors of [7, 13] provide also lower bounds of α_n for $n \leq 15$. In particular, they show that $\alpha > \frac{4}{3}$, since they prove (compute) that $\alpha_n \geq \frac{11}{8}$ for $n = 9$. Lower bounds were also provided by Charikar et al. [9] for arbitrarily large n, but they are rather weak for $n \leq 25$. We remark that the literature is more extensive for the Symmetric TSP [5, 20, 21, 32, 33]. For instance, [21, 32, 33] propose STSP instances that have a large integrality gap and are hard to solve for the state-of-the-art STSP solver Concorde [1]. However, no theoretical proof is available for the exact value of the integrality gap, neither for the STSP nor the ATSP. Furthermore, the relation between computational complexity and large integrality gap is still unclear even in the symmetric case.

Main contributions. This paper has three main contributions. First, we identify, for the first time, a group of symmetries of the ASEP polytope. We exploit this symmetry to design pivoting strategies that explore vertices of P^n_{ASEP}. Second, we provide new lower bounds for the integrality gap α_n for the ATSP for $16 \leq n \leq 22$ by using a new pivoting algorithm which exploits the symmetries of the vertices of P^n_{ASEP}, combined with an inductive algorithm that generates vertices of P^{n+1}_{ASEP} from a vertex of P^n_{ASEP}. Our bounds improve those provided in [9] and [13]. Third, by using our new inductive algorithm, we generate hard ATSP instances, where complexity is measured with respect to the Concorde solver for STSP [1] after an appropriate transformation of the ATSP instance, and with respect to two dedicated ATSP solvers [14, 16].

The outline of this paper is as follows. Section 2 reviews the background material. Section 3 studies the symmetries of the polytope P^n_{ASEP}. In Section 4, we explain how we use the algebraic structure introduced to perform a symmetry-breaking heuristic pivoting. Furthermore, we introduce a new operator that generates vertices of P^{n+1}_{ASEP} from a vertex of P^n_{ASEP}. In Section 5 we present the results of our approach, by analyzing the structure of the obtained vertices and exhibiting new lower bounds for $16 \leq n \leq 22$. Finally, in Section 6 we conclude the paper with a perspective on future works.

2 Background material

A key subproblem of our approach is the computation of the maximum integrality gap over all possible pseudo-quasi metric cost vectors $\boldsymbol{c} \in \mathbb{R}^m_+$ for a single vertex of the ASEP polytope. This subproblem was first introduced in [5] for the STSP and later in [13] for the ATSP. The main idea is to divide the cost vector $\boldsymbol{c}$ by the optimal value ATSP($\boldsymbol{c}$), obtaining $\boldsymbol{c'}$ such that ATSP($\boldsymbol{c'}$) $= 1$. This transformation leaves unchanged any tour leading to an optimal solution. Hence, one can consider without loss of generality the definition of IG as to $\alpha_n := \sup_{\boldsymbol{c} \text{ s.t ATSP}(\boldsymbol{c})=1} \frac{1}{\text{ASEP}(\boldsymbol{c})}$, which is equivalent to solve $\inf_{\boldsymbol{c} \text{ s.t ATSP}(\boldsymbol{c})=1}$ ASEP($\boldsymbol{c}$). Note that the operation of dividing the costs by ATSP($\boldsymbol{c}$) maintains the triangle inequalities and preserves the value of the IG.

The problem of computing the maximum α_n of K_n for the pseudo-quasi metric (pq-metric) ATSP is as follows [13].

$$\frac{1}{\alpha_n} := \min_{\substack{\boldsymbol{c} \text{ is pq-metric,} \\ \text{ATSP}(\boldsymbol{c})=1}} \text{ASEP}(\boldsymbol{c}) = \min_{\boldsymbol{x} \in P^n_{ASEP}} \min_{\substack{\text{is pq-metric,} \\ \text{ATSP}(\boldsymbol{c})=1}} \boldsymbol{x}^T \boldsymbol{c}. \tag{8}$$

To solve the problem (8) for a fixed (small) value of n, the authors in [13] enumerate the vertices of P^n_{ASEP}, and for each vertex $\boldsymbol{x} \in P^n_{ASEP}$, they solve $\min \{ \boldsymbol{c}^T \boldsymbol{x} \mid \boldsymbol{c} \text{ is pq-metric, ATSP}(\boldsymbol{c}) = 1 \}$. In [13], the latter inner problem is called Gap($\boldsymbol{x}$). Intuitively, Gap($\boldsymbol{x}$) allows us to determine, among all cost vectors that have an optimal ASEP solution at point $\boldsymbol{x}$, the one that results in the largest integrality gap. Since the number of vertices of P^n_{ASEP} is finite, we only need to explore a fixed number of cases. With a slight abuse of notation, we refer to “the integrality gap of a vertex” as the integrality gap induced by the cost vector that maximizes the integrality gap among those with an optimal ASEP solution at $\boldsymbol{x}$.

The definition of Gap$(\boldsymbol{x})$ relies heavily on the slackness compatibility conditions, which ensure that an optimal primal-dual pair satisfies complementary slackness.

For this reason, the definition of Gap$(\boldsymbol{x})$ involves the dual variables of the linear formulation (2)–(4), where $\boldsymbol{x} \geq 0$. Let y_j^{in} and y_i^{out} be the dual variables associated with the in-degree constraint (2) and out-degree constraint (3), respectively. Let d_S be the dual variables associated with the subtour elimination constraint (4). Finally, let c_{ij} denote the cost variable on arc (i, j). The function Gap$(\boldsymbol{x})$ is defined as below. For further details, the interested reader can check [13].

$$
\begin{aligned}
\text{Gap}(\boldsymbol{x}) := \min & \sum_{(i,j)\in A} x_{ij} c_{ij} && (9)\\
\text{s.t.} & \sum_{(i,j)\in A} z_{ij} c_{ij} \geq 1 \quad \forall \boldsymbol{z} \in \mathcal{T}^n_{ASEP} && (10)\\
& c_{ij} \leq c_{ik} + c_{jk} \quad \forall i, j, k \in V && (11)\\
& c_{ij} \geq 0 \quad \forall (i, j) \in A && (12)\\
& c_{ij} - y_i^{\text{out}} - y_j^{\text{in}} - \sum_{S\in\mathcal{S}_{ij}(\boldsymbol{x})} d_S \geq 0 \quad \forall (i, j) \in A \backslash A(\boldsymbol{x}) && (13)\\
& c_{ij} - y_i^{\text{out}} - y_j^{\text{in}} - \sum_{S\in\mathcal{S}_{ij}(\boldsymbol{x}^*)} d_S = 0 \quad \forall (i, j) \in A(\boldsymbol{x}) && (14)\\
& d_S \geq 0 \quad \forall S \in \bigcup_{(i,j)\in A} \mathcal{S}_{ij}(\boldsymbol{x}), && (15)
\end{aligned}
$$

where $\mathcal{T}^n_{\text{ASEP}}$ is the collection of every possible Hamiltonian cycle of K_n, and $\boldsymbol{z} \in \{0, 1\}^m$ are incidence vectors of elements of $\mathcal{T}^n_{\text{ASEP}}$. We remark that the variables are c_{ij}, $y_i^{\text{in}}, y_i^{\text{out}}, d_S$, while $\boldsymbol{x}, \boldsymbol{z}$ are given. Constraints (10) ensure that the optimal solution $\boldsymbol{c}^*$ of Gap$(\boldsymbol{x})$ yields ATSP$(\boldsymbol{c}^*) = 1$. Constraints (13)–(15) derive from dualizing the linear program relaxation of (2)–(4). Here, we define the following subset of nodes $S_{ij(\boldsymbol{x})}$ and of arcs $A(\boldsymbol{x})$ as follows: $\mathcal{S}_{ij}(\boldsymbol{x}) = \{S \subset A | (i, j) \in \delta(S), \boldsymbol{x}(\delta(S)) = 1, 2 \leq |S| \leq n - 2\}$ and $A(\boldsymbol{x}) = \{(i, j) \in A \mid x_{ij} > 0\}$. Constraints (13)–(15) ensure that

$$
\boldsymbol{x}^* \in \arg \min_{\boldsymbol{x}\in P^n_{ASEP}} \boldsymbol{c}^*\boldsymbol{x} \Leftrightarrow \boldsymbol{c}^* \in \arg \min_{\boldsymbol{c},\boldsymbol{y},\boldsymbol{d} \text{ satisfy (10)–(15)}} \text{Gap}(\boldsymbol{x}^*).
$$

Thus, the $\arg\min \boldsymbol{c}^*$ of the program Gap$(\boldsymbol{x}^*)$ is such that, once ASEP$(\boldsymbol{c}^*)$ is solved, the minimum is attained precisely at $\boldsymbol{x}^*$ (for details, see [13]).

3 Symmetry group of P^n_{ASEP}

Polyhedral aspects of the TSP have been extensively studied in the past decades. In particular, in [**grotschelbook**, 4, 26] the polyhedral properties of the convex hull of the integer vertices, the so-called "natural polytope", of the STSP and the ATSP have been investigated starting from the assignment polytope. More specifically, it has been shown that the diameter of the assignment polytope is two, which in turn implies that the diameter of the TSP polytope is at most 2. However, since the valid formulation for the TSP examined in this paper – namely, the one proposed by Dantzig, Fulkerson, and Johnson [12] – is not integral, our focus is on the relationship between optimizing only on the integer points and optimizing over P^n_{ASEP} (linear relaxation). In this section, we focus in particular on the fractional vertices and the symmetry properties of the subtour elimination polytope P^n_{ASEP}.

As remarked in [13], the vertices of P^n_{ASEP} can be subdivided into equivalence classes through permutations of the nodes of K_n. In this section, we define explicitly a symmetry group of P^n_{ASEP} based on permutations. The classes of isomorphic vertices turn out to be the orbits generated by this symmetry group.

By observing the definition of P^n_{ASEP}, an important consideration can be made: Due to the structure of the constraints, they are not affected by a permutation of the node indices. More precisely, it is well known that any relabeling of the nodes $i \in V$ induces just an internal permutation of the constraint groups (2), (3), and (4), which leaves the feasible region unchanged. Consequently, it is possible to identify a group of symmetries of the polytope P^n_{ASEP} induced by the symmetric group S_n of permutations of the nodes $i \in V$. To describe the symmetries of P^n_{ASEP} explicitly, it is useful to convert the feasible solutions into matrix form. More precisely, we can rewrite any feasible solution $\boldsymbol{x} \in P^n_{ASEP}$ as a matrix $\boldsymbol{X} \in [0,1]^{n\times n}$, with the corresponding components x_{ij} for $i \neq j$ and setting $x_{ij} = 0$ for $i = j$.

Now, consider the symmetric group of permutations on n elements S_n. Let $\pi \in S_n$, such that $\pi : i \mapsto \pi(i)$, be a permutation of the nodes $i \in V$. For any feasible solution $\boldsymbol{x} \in P^n_{ASEP}$, with matrix representation $\boldsymbol{X}$, it is possible to generate a new feasible solution $\boldsymbol{x'}$, expressed by a matrix $\boldsymbol{X'}$, by applying the permutation π to the nodes of the graph K_n. It must hold

$$x'_{\pi(i)\pi(j)} = x_{ij} \quad \forall i, j \in V. \tag{16}$$

This means that $\boldsymbol{X'}$ is obtained by permuting rows and columns of $\boldsymbol{X}$ according to π. Given a permutation of n elements $\pi \in S_n$, let us recall the definition of *permutation matrix* as the matrix $\boldsymbol{P}_\pi = (p_{ij})$ such that

$$p_{ij} = \begin{cases} 1 & \text{if } i = \pi(j) \\ 0 & \text{otherwise.} \end{cases}$$

In the product $\boldsymbol{P_\pi X}$, the permutation matrix $\boldsymbol{P_\pi}$ permutes the rows of $\boldsymbol{X}$ according to π. Since also the columns of $\boldsymbol{X}$ have to be permuted, we apply $\boldsymbol{P_\pi}$ to the transpose of $\boldsymbol{P_\pi X}$. Thus

$$\boldsymbol{X'} = \left(\boldsymbol{P_\pi}(\boldsymbol{P_\pi X})^T\right)^T = (\boldsymbol{P_\pi X})\boldsymbol{P_\pi}^T = \boldsymbol{P_\pi X P_\pi}^T.$$

A notion that we will widely use is the *isomorphism between digraphs.* Hence, let us recall some helpful definitions.

Definition 1 (Support digraph)**.** *Let $\boldsymbol{x} \in P^n_{ASEP}$. The weighted support digraph $\boldsymbol{x}$ is the graph $H(\boldsymbol{x})$ defined on the set of nodes V, having an arc (i, j) with the weight x_{ij}, if and only if $x_{ij} > 0$.*

Definition 2 (Isomorphism between weighted graphs)**.** *Two graphs $D = (V, A_D)$ and $F = (V, A_F)$ on n nodes are isomorphic if there exists a permutation π of V such that $(u, v) \in A_D \iff (\pi(u), \pi(v)) \in A_F$. Furthermore, the weights $\mathbf{c}^D, \mathbf{c}^F$ of the edges must satisfy $c^F_{\pi(u)\pi(v)} = c^D_{uv}, \forall u, v \in V$.*

Example 1. *Consider $\boldsymbol{x} \in P^4_{ASEP}$ defined by*

$$\boldsymbol{x} = \left(\frac{1}{2}, 0, \frac{1}{2}, \frac{1}{2}, \frac{1}{2}, 0, \frac{1}{2}, 0, \frac{1}{2}, 0, \frac{1}{2}, \frac{1}{2}\right)^T.$$

Its matrix version is hence

$$\boldsymbol{X} = \begin{pmatrix} 0 & \frac{1}{2} & 0 & \frac{1}{2} \\ \frac{1}{2} & 0 & \frac{1}{2} & 0 \\ \frac{1}{2} & 0 & 0 & \frac{1}{2} \\ 0 & \frac{1}{2} & \frac{1}{2} & 0 \end{pmatrix}.$$

This feasible solution is associated with the support graph in Figure 1, left. Let $\pi = (0\ 1\ 2\ 3)$, that is the permutation such that $\pi(0) = 1,\ \pi(1) = 2,\ \pi(2) = 3,\ \pi(3) = 0$. Thus, in this case

$$\boldsymbol{P}_\pi = \begin{pmatrix} 0 & 0 & 0 & 1 \\ 1 & 0 & 0 & 0 \\ 0 & 1 & 0 & 0 \\ 0 & 0 & 1 & 0 \end{pmatrix}$$

and we obtain

$$\boldsymbol{X'} = \boldsymbol{P}_\pi \boldsymbol{X} \boldsymbol{P}_\pi^T = \begin{pmatrix} 0 & 0 & \frac{1}{2} & \frac{1}{2} \\ \frac{1}{2} & 0 & \frac{1}{2} & 0 \\ 0 & \frac{1}{2} & 0 & \frac{1}{2} \\ \frac{1}{2} & \frac{1}{2} & 0 & 0 \end{pmatrix},$$

which corresponds to the graph in Figure 1 on the right.

For any node relabeling $\pi \in S_n$ we can define the corresponding permutation of a solution $\boldsymbol{X}$ as

$$\begin{aligned} g_\pi : [0,1]^{n\times n} &\to [0,1]^{n\times n} \\ \boldsymbol{X} &\mapsto \boldsymbol{P}_\pi \boldsymbol{X} \boldsymbol{P}_\pi^T. \end{aligned} \tag{17}$$

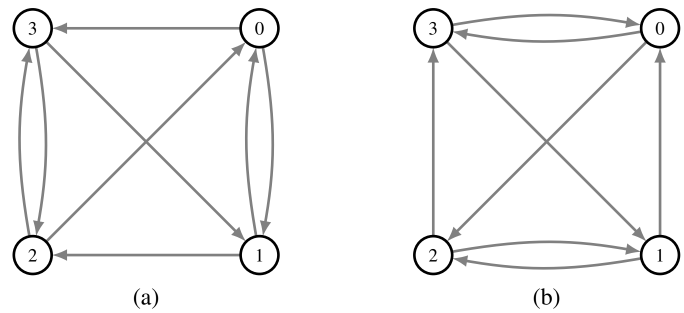

Figure 1: Two isomorphic vertices obtained via vertex permutation. Each arc is weighted $\frac{1}{2}$.

With a slight abuse of notation, we will use both $g_\pi(\boldsymbol{x})$ and $g_\pi(\boldsymbol{X})$ interchangeably, denoting the *row and column permutation* of $\boldsymbol{X}$, according to π.

First of all, we observe that the map is well defined in P^n_{ASEP}, namely $\boldsymbol{x} \in P^n_{ASEP}$ implies $g_\pi(\boldsymbol{x}) \in P^n_{ASEP}$. Hence, all the constraints are satisfied also for $g_\pi(\boldsymbol{x})$ by a simple "shuffle" of the rows: degree constraints i become degree constraints $\pi(i)$ and subtour elimination constraints associated to $\delta(S),\ S = \{s_1, \dots, s_r\}$ become $\delta(\pi(S)),\ \pi(S) := \{\pi(s_1), \dots, \pi(s_r)\}$. The isomorphism of vertices, observed in [13], can now be extended to the whole polytope P^n_{ASEP}. Hence, it trivially follows

Lemma 1. *Let $x \in P^n_{ASEP}$ and $\pi \in S_n$. The support graphs $H(\boldsymbol{x})$ and $H(g_\pi(\boldsymbol{x}))$ are isomorphic.*

Let $G(n) = \{g_\pi \mid \pi \in S_n\}$ be the set of all transformations g_π. The next theorem shows that $G(n)$ is a group of symmetries of the polytope.

Theorem 2. *$G(n)$ is a group of isometries acting on of P^n_{ASEP}.*

Proof. We begin by showing the closure of $G(n)$ under composition. Let $\pi_1, \pi_2 \in S_n$. By equation (17) we have

$$\begin{aligned} g_{\pi_1} g_{\pi_2}(\boldsymbol{X}) &= g_{\pi_1}\left(\boldsymbol{P}_{\pi_2} \boldsymbol{X} \boldsymbol{P}^T_{\pi_2}\right) = \boldsymbol{P}_{\pi_1} \boldsymbol{P}_{\pi_2} \boldsymbol{X} \boldsymbol{P}^T_{\pi_2} \boldsymbol{P}^T_{\pi_1} \\ &= \left(\boldsymbol{P}_{\pi_1\pi_2}\right) \boldsymbol{X} \left(\boldsymbol{P}_{\pi_1\pi_2}\right)^T = g_{\pi_1\pi_2}(\boldsymbol{X}) \in G(n). \end{aligned} \tag{18}$$

It is not difficult to verify that the symmetric group S_n induces the group structure on $G(n)$. In particular, by equation (18) we have that the identity element of $G(n)$ is g_{id} and the inverse element of g_π is $g_{\pi^{-1}}$. Moreover, equation (18) states that $G(n)$ and S_n are isomorphic groups. By equation (16) it can be observed that for any feasible solution $\boldsymbol{x} \in P^n_{ASEP}$ the solution $\boldsymbol{x}' = g_\pi(\boldsymbol{x}) \in P^n_{ASEP}$ is obtained by a permutation of the components of $\boldsymbol{x}$ based on π. Therefore, it is immediately clear that g_π preserves the Euclidean distance, that is $||g_\pi(\boldsymbol{x}) - g_\pi(\boldsymbol{y})|| = ||\boldsymbol{x} - \boldsymbol{y}||\ , \forall \boldsymbol{x}, \boldsymbol{y} \in P^n_{ASEP}, \pi \in S_n$. ◻

As explained in Section 2, our main goal is the computation of the integrality gap of vertices. The following corollary focuses on the action of $G(n)$ on the set of vertices, which will be denoted throughout the manuscript with $\mathcal{X}^n_{ASEP}$.

Corollary 3. *Let $\boldsymbol{x} \in \mathcal{X}^n_{ASEP}$ and $g_\pi \in G(n)$. Then $g_\pi(\boldsymbol{x}) \in \mathcal{X}^n_{ASEP}$.*

Proof. g_π is an isometry and isometries map vertices into vertices. ◻

Since the group $G(n)$ acts on the set of vertices $\mathcal{X}^n_{ASEP}$, it is of interest to study the *orbit* of each vertex $\boldsymbol{x} \in \mathcal{X}^n_{ASEP}$, that is the set

$$O_{\boldsymbol{x}} = \{g_\pi(\boldsymbol{x}) \mid g_\pi \in G(n)\}, \tag{19}$$

and the *stabilizer* of $G(n)$ with respect to $\boldsymbol{x} \in \mathcal{X}^n_{ASEP}$, that is the subgroup of $G(n)$ defined as

$$G_{\boldsymbol{x}} = \{g_\pi \in G(n) \mid g_\pi(\boldsymbol{x}) = \boldsymbol{x}\}.$$

Combining Lemma 1 and (19), we can conclude that vertices of the polytope P^n_{ASEP} belonging to the same orbit have isomorphic support graphs. In other terms, the isomorphism classes of vertices introduced in [13] are the orbits of the vertices with respect to the group $G(n)$.

By the so-called *orbit-stabilizer theorem* we have the relation $|G(n)| = |G_{\boldsymbol{x}}||O_{\boldsymbol{x}}|$. Further details on the orbit-stabilizer theorem can be found, for instance, in [2]. A natural question concerns the role of the stabilizer of each vertex, and whether it leads to some implications in combinatorial questions, such as the integrality gap. For example, what could be the relationship between the stabilizer of a vertex and the maximum integrality gap achievable at that vertex? The case of the integer vertices is particularly interesting. As already pointed out, integer vertices of P^n_{ASEP} correspond to Hamiltonian cycles of K_n. However, Hamiltonian cycles differ from each other only by a relabeling of the nodes. Therefore, we can prove the following property.

Lemma 4. *Let $\boldsymbol{x} \in \mathcal{T}^n_{ASEP}$. Then, it holds $O_{\boldsymbol{x}} = \mathcal{T}^n_{ASEP}$.*

Proof. Let $\boldsymbol{x_1}, \boldsymbol{x_2} \in \mathcal{T}^n_{ASEP}$. Since $\boldsymbol{x_1}$ and $\boldsymbol{x_2}$ correspond to Hamiltonian cycles in K_n, there exists a permutation π, such that $g_\pi(\boldsymbol{x_1}) = \boldsymbol{x_2}$. It follows that $\boldsymbol{x_1}$ and $\boldsymbol{x_2}$ belong to the same orbit of $G(n)$. □

A consequence of Lemma 4 is that integer vertices build a unique orbit $O_{\boldsymbol{x}}$ with $|O_{\boldsymbol{x}}| = (n-1)!$. By the orbit-stabilizer theorem it follows that $|G_{\boldsymbol{x}}| = n, \ \forall \boldsymbol{x} \in \mathcal{T}^n_{ASEP}$.

More specifically, it holds the following.

Lemma 5. *If $\boldsymbol{x} \in \mathcal{T}^n_{ASEP}$, then $G_{\boldsymbol{x}}$ is the group*

$$\langle (1\ 2 \ldots n) \rangle$$

of all the cyclic permutations that are

$$\tau_k(i) = (i + k) \mod n.$$

Proof. As these permutations are the k-shift of nodes, $k \in \{0, 1, 2, \ldots, n\}$, it holds

$$\tau_{k_1} \circ \tau_{k_2} = \tau_{k_3} \qquad k_3 = (k_1 + k_2) \mod n.$$

□

Unfortunately, as further discussed in Section 5.3, the stabilizer of a fractional vertex $\boldsymbol{x}$ of P^n_{ASEP} does not seem to follow a general recipe.

In Section 6, we conjecture that vertices having a large integrality gap are the ones having large but not trivial stabilizers; hence, it could be relevant to know in advance the structure of the stabilizer to guess the "promising" vertices.

It is worth remarking that the orbits of $G(n)$ form large classes of isomorphic vertices; hence, P^n_{ASEP} can be considered a highly symmetric polytope.

The intrinsic equivalence of vertices belonging to the same orbit is visible in the following lemma.

Lemma 6. *Let $\boldsymbol{x}, \boldsymbol{y} \in \mathcal{X}^n_{ASEP}$ such that $\boldsymbol{y} \in O_{\boldsymbol{x}}$, then $Gap(\boldsymbol{x}) = Gap(\boldsymbol{y})$.*

Proof. If $\boldsymbol{x}, \boldsymbol{y} \in O_{\boldsymbol{x}}$, then there exists $g_\pi \in G(n)$, such that $\boldsymbol{x} = g_\pi(\boldsymbol{y})$. Let $\boldsymbol{c}^* \in \arg\min Gap(\boldsymbol{x})$.

$$Gap(\boldsymbol{x}) = \boldsymbol{c}^{*T}\boldsymbol{x} = g_\pi(\boldsymbol{c}^*)^T g_\pi(\boldsymbol{x}) = Gap(\boldsymbol{y}).$$

The first equation holds by definition, while the second equation remains unchanged even if both terms of the scalar product are permuted. The final equation is derived from the fact that if there exists a $\boldsymbol{c}'$ value such that $\boldsymbol{c'}^T\boldsymbol{x}' < \boldsymbol{c^*}^T\boldsymbol{x}$, then $g_\pi^{-1}(\boldsymbol{c}')$ would provide a solution of lower cost than $\boldsymbol{c^*}^T$, thus rendering the latter non-optimal. □

Note that this result has already been proved in [13], using a different strategy. Finally, we add a result that justifies our symmetry-breaking simplex algorithm presented in the next section.

Definition 3. *The set of all vertices adjacent to $\boldsymbol{x} \in \mathcal{X}^n_{ASEP}$ is called the* **neighborhood of** $\boldsymbol{x}$ *and is denoted by $\mathcal{N}(\boldsymbol{x})$.*

Lemma 7. *Let $\boldsymbol{x}, \boldsymbol{y} \in \mathcal{X}^n_{ASEP}$, $\pi \in S_n$. Then, $\boldsymbol{y} \in \mathcal{N}(\boldsymbol{x}) \Leftrightarrow g_\pi(\boldsymbol{y}) \in \mathcal{N}(g_\pi(\boldsymbol{x}))$.*

Proof. First, we use the transformation π to sort the rows of the constraint matrix, by mapping each degree constraint associated with i to $\pi(i)$, and each subtour elimination constraint associated with $S = \{s_1, \ldots, s_f\}$ to $\pi(S) := \{s_1, \ldots, s_f\}$ and each non-negative constraint accordingly. With a slight abuse of notation, we will call $\pi(i)$ the mapping of the i^{th} constraint. Note that $\boldsymbol{y}$ shares exactly $r(n) - 1$ linearly independent and tight constraints with $\boldsymbol{x}$, let $i_1, \ldots, i_{n_y - 1}, i_{n_y}$ are this set of constraints of $\boldsymbol{y}$ and $i_1, \ldots, i_{n_y-1}, i_{n_x}$ is the one of $\boldsymbol{x}^3$, then, $\pi(i_1), \ldots, \pi\left(i_{n_y-1}\right), \pi\left(i_{n_y}\right)$ is associated to $g_\pi(\boldsymbol{y}$ and $\pi(i_1), \ldots, \pi\left(i_{n_y-1}\right), \pi\left(i_{n_x}\right)$ is hence associated with $g_\pi(\boldsymbol{x})$. Thus, $g_\pi(\boldsymbol{y}) \in \mathcal{N}(g_\pi)(\boldsymbol{x}))$. □

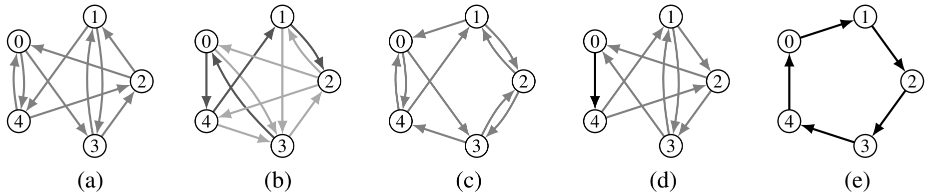

Figure 2: Support graphs of the 5 isomorphism classes for $n = 5$. The arcs have a grey level depending on the value of the corresponding x_i. See Table 2 for details: while (a) and (c) have all $x_i = \frac{1}{2}$ (light grey); in the support graph (b) 4 arcs correspond to $x_i = \frac{2}{3}$ (dark grey) and 7 to $x_i = \frac{1}{3}$; (d) 8 arcs have $x_i = \frac{1}{2}$ and 1 arc $x_i = 1$; (e) all $x_i = 1$.

Substantially, Lemma 7 states that the maps g_π preserve the adjacency of vertices. In other words, vertices belonging to the same orbit are equivalent also in terms of their neighborhoods.

4 Computing vertices with a large integrality gap

The orbits of the vertices of P^n_{ASEP} introduced in the previous section are here used to design a computational strategy for heuristically generating vertices of P^n_{ASEP}. In the next paragraphs, first, we introduce our pivoting algorithm that exploits the vertex symmetries to avoid the exploration of isomorphic vertices. Then, we introduce a new iterative procedure that generates vertices of P^{n+1}_{ASEP} starting from vertices of P^n_{ASEP}.

4.1 Pivoting by symmetry-breaking

In this subsection, we illustrate the new pivoting algorithm, which attempts to avoid the exploration of new vertices that are isomorphic to vertices already visited. The pivoting algorithm will be denoted by Pivoting$(\boldsymbol{x}, T)$, where the meaning of the variable T will be clarified later.

The main idea is simple: we start with a basic feasible solution, that is a vertex $\boldsymbol{x} \in P^n_{ASEP}$, and we explore all vertices in the neighborhood $\mathcal{N}(\boldsymbol{x})$ one at a time, by enumerating (or by sampling) the possible pivoting steps for that vertex. If the new vertex obtained by pivoting is not isomorphic to any vertex already explored, then we solve the optimization problem (9)–(15) to find the maximal integrality gap for that new vertex, and we record the corresponding orbit. We iterate the neighborhood search either with a complete enumeration for small values of n (e.g., $n \leq 8$), or with a random sampling strategy for $n > 8$. Our procedure is iterative, namely, it continues to iterate vertex-by-vertex, exploring each time the neighborhood of each vertex. The input parameters are:

- M, the maximum number of iterations of the algorithm, equivalent to the maximum number of vertices we pivot on.
- T_{tot}, timelimit for the whole iterations.
- T_{it}, timelimit for a single iteration.

Parameter T_{it} balance the tradeoff between *exploration* and *exploitation*. Small values of T_{it} allow for exploring only a few elements adjacent to a given vertex $\boldsymbol{x}$ and quickly moving on to the next neighboring vertex to be explored. On the other hand, high values of T_{it} insist heavily on the neighborhood of a vertex $\boldsymbol{x}$. We continue to iterate the procedure until either the timelimit T_{tot} is hit or the maximum number M of iterations is reached.

We named this algorithm "explore/exploit" for two reasons: the parameter T_{it} governs the exploitation of a single vertex. For small values of T_{it}, we do not focus much on the neighborhood of a single vertex, instead preferring to pivot on multiple vertices. However, for large values of T_{it}, we continue to build a single $\mathcal{N}(\boldsymbol{x})$, having less time to explore different areas of P^n_{ASEP}.

Hence, given a time limit of T, our function

$$\mathcal{N}'(\boldsymbol{x}) = \text{Pivoting}(\boldsymbol{x}, T) \tag{20}$$

returns only a subset of $\mathcal{N}(\boldsymbol{x})$, namely the adjacent vertices that the strategy is capable of finding within a time limit.

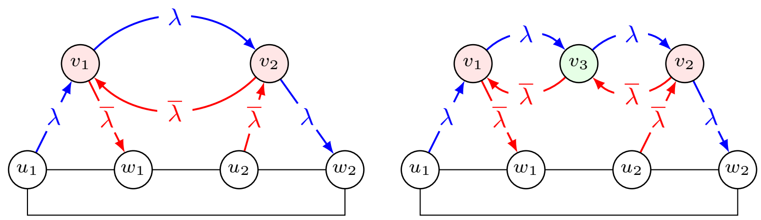

(a) Vertex $\boldsymbol{x} \in P^n_{ASEP}$. (b) New vertex $\boldsymbol{x} \in P^{n+1}_{ASEP}$.

Figure 3: Example of λ-loop breaking $(\boldsymbol{x} \uparrow^{v_3} (v_1, v_2))_{uv}$, with $\overline{\lambda} = 1 - \lambda$.

4.2 Generating vertices using loop breaking procedure

In this subsection, we present our new iterative algorithm to compute a vertex of P^{n+1}_{ASEP} by starting from a vertex of P^n_{ASEP}. First, we recover two definitions and a lemma from [13] that we use to prove our new result. Then, we introduce our loop-breaking procedure.

Definition 4 ([13], Chap. 3)**.** *Let $S \subset V$ and $\boldsymbol{x} \in P^n_{ASEP}$. If $\delta(\boldsymbol{x}(S)) := \sum_{(i,j)\in\delta(S)} x_e = 1$, then, S is called a* ***tight set****.*

Note that a tight set is a subset of vertices that induces a cut that satisfies a subtour elimination constraint with equality.

Definition 5 ([13], Chap. 3)**.** *Let $S \subset V$ be a tight set and $\boldsymbol{x} \in P^{n+|S|-1}_{ASEP}$. Then, we can collapse the set S into node w as follows:*

$$(\boldsymbol{x} \downarrow_w (S))_{uv} = \begin{cases} \sum_{s\in S} x_{us} & \textit{if } v = w, \\ \sum_{s\in S} x_{sv} & \textit{if } u = w, \\ x_{uv} & \textit{otherwise.} \end{cases}$$

Lemma 8 ([13], Prop. 3.3.1)**.** *Let $\boldsymbol{x} \in P^n_{ASEP}$ and $S \subset V$ be a tight set of $\boldsymbol{x}$. Then, $\boldsymbol{x} \downarrow_w (S)$ belongs to $P^{n-|S|+1}_{ASEP}$.*

We are now ready to formally introduce λ-loops.

Definition 6 (λ-loop)**.** *Let $\boldsymbol{x} \in P^n_{ASEP}$ and let $v_1, v_2 \in V$ such that $x_{v_1 v_2} = \lambda$ and $x_{v_2 v_1} = 1 - \lambda$, then, we say that $\boldsymbol{x}$* ***contains a λ-loop*** *$\overleftrightarrow{v_1 v_2}$.*

The following trivially follows.

Lemma 9. *Consider $\boldsymbol{x}$ a point in P^n_{ASEP} containing the λ-loop $\overleftrightarrow{v_1 v_2}$, then $S = \{v_1, v_2\}$ is a tight set.*

Proof. The amount of flow entering v_1 is λ, while the amount of flow entering v_2 is $1 - \lambda$. Hence, $\boldsymbol{x}(\delta(S)) = 1$. $\square$

4.2.1 A new λ-loop breaking procedure

Our algorithm for generating vertices of P^{n+1}_{ASEP} from P^n_{ASEP} exploits λ-loop in the following λ-loop breaking procedure.

Definition 7. *Let $\boldsymbol{x} \in P^n_{ASEP}$ that contains a λ-loop $\overleftrightarrow{v_1 v_2}$. Then, the* ***$\lambda$-loop breaking procedure*** *generates a point in $\mathbb{R}^{(n+1)n}$ adding the node v_3 as follows :*

$$(\boldsymbol{x} \uparrow^{v_3} (v_1, v_2))_{uv} = \begin{cases} \lambda & \textit{if } uv \in \{v_1 v_3,\ v_3 v_2\}, \\ 1 - \lambda & \textit{if } uv \in \{v_3 v_1,\ v_2 v_3\}, \\ 0 & \textit{if } uv \in \{v_1 v_2,\ v_2 v_1\} \\ 0 & \textit{if } v = v_3 \textit{ and } u \notin \{v_1, v_2\} \\ x_{uv} & \textit{otherwise.} \end{cases}$$

The λ-loop breaking procedure has the following properties.

Lemma 10. *$S = \{v_1, v_3\}$ is a tight set for $\boldsymbol{x} \uparrow^{v_3} (v_1, v_2)$.*

Proof. Let $\boldsymbol{x}' = \boldsymbol{x} \uparrow^{v_3} (v_1, v_2)$

$$\boldsymbol{x}'(\delta(S)) = \sum_{\substack{b\in V \\ b\neq v_3}} x_{v_1 b} + \sum_{\substack{b\in V \\ b\neq v_1}} x_{v_3 b}$$

given that

$$\sum_{b\in V} x_{v_1 b} = 1 \Rightarrow \sum_{\substack{b\in V\\ b\neq v_3}} x_{v_1 b} = 1 - x_{v_1 v_3} = 1-\lambda,$$
$$\sum_{b\in V} x_{v_3 b} = 1 \Rightarrow \sum_{\substack{b\in V\\ b\neq v_1}} x_{v_3 b} = 1 - x_{v_3 v_1} = 1-(1-\lambda) = \lambda,$$
$$\Rightarrow \boldsymbol{x}'(\delta(S)) = 1-\lambda+\lambda = 1.$$

□

Lemma 11. *If $\boldsymbol{x}$ is a vertex of P^n_{ASEP} that contains a λ-loop $\overleftrightarrow{v_1 v_2}$, then $\boldsymbol{x} \uparrow^{v_3} (v_1, v_2)$ is a vertex of P^{n+1}_{ASEP}.*

Proof. Let $\boldsymbol{x}' := \boldsymbol{x} \uparrow^{v_3} (v_1, v_2)$. Clearly $\boldsymbol{x}'$ is feasible. To show that $\boldsymbol{x}$ is also a vertex, assume by contradiction that there exists $\boldsymbol{y}', \boldsymbol{z}' \in P^{n+1}_{ASEP}$ and $\mu \in (0,1)$ such that $\boldsymbol{x}' = \mu\boldsymbol{y}' + (1-\mu)\boldsymbol{z}'$. Let $S = \{v_1, v_3\}$. Note that

$$\boldsymbol{x}'(\delta(S)) = 1 = \mu\boldsymbol{y}'(\delta(S)) + (1-\mu)\boldsymbol{z}'(\delta(S)). \tag{21}$$

As $\boldsymbol{y}', \boldsymbol{z}'$ are feasible, we have $\boldsymbol{y}'(\delta(S)) \geq 1$ and $\boldsymbol{z}'(\delta(S)) \geq 1$. As the equality should hold, we have then $\boldsymbol{z}'(\delta(S)) = \boldsymbol{y}'(\delta(S)) = 1$. Thus, we have

$$\boldsymbol{y} :=\downarrow_{v_1} \boldsymbol{y}'(S) \quad \text{and} \quad \boldsymbol{z} :=\downarrow_{v_1} \boldsymbol{z}'(S).$$

Thanks to Lemma 8, $\boldsymbol{z}, \boldsymbol{y} \in P^n_{ASEP}$. Clearly, $\boldsymbol{x} = \mu\boldsymbol{y} + (1-\mu)\boldsymbol{z}$. This can be verified entry by entry. As an example, consider the case $e = uv_1$:

$$\begin{aligned} \mu y_{uv_1} + (1-\mu) z_{uv_1} &= \mu\left(y'_{uv_1} + y'_{uv_3}\right) + (1-\mu)\left(z'_{uv_1} + z'_{uv_3}\right) \\ &= \left[\mu y'_{uv_1} + (1-\mu) z'_{uv_1}\right] + \left[\mu y'_{uv_3} + (1-\mu) z'_{uv_3}\right] \\ &= x'_{uv_1} + x'_{uv_3} = x_{uv_1}. \end{aligned}$$

Thus, $\boldsymbol{x}$ is not a vertex of P^n_{ASEP}, and we get a contradiction. □

Remark 1. *Note that the converse unfortunately does not hold, e.g., if you collapse a λ-loop into a single node, you are not guaranteed to obtain a vertex. This will be particularly relevant in Section 5.4 where we collapse instead λ-loops: after doing that, we have to check that what we obtain is again a vertex. However, it always leads to a feasible point thanks to Lemma 8.*

4.2.2 How we used this procedure

If we are able to compute an initial vertex $\boldsymbol{x}_0 \in P^n_{ASEP}$ having a $\lambda-$loop, then, we can iteratively apply the λ-loop breaking procedure to obtain a sequence of vertices $\boldsymbol{x}_1, \boldsymbol{x}_2, \ldots, \boldsymbol{x}_t$ that belongs to $P^{n+1}_{ASEP}, P^{n+2}_{ASEP}, \ldots, P^{n+t}_{ASEP}$, respectively. Note that a similar idea was explored in [13], where the author introduced a *2-jack insertion* procedure, where a node satisfying precise hypotheses is replaced with a λ-loop, with the strict condition $\lambda = \frac{1}{2}$. Our strategy is more general since we allow any value of $\lambda \in (0,1)$. Our experimental results show that our procedure is very effective in finding vertices with large integrality gaps (see Section 5.1).

4.3 The full algorithm

For a formal description of the proposed procedure, see Algorithm 1. The Pivoting function mentioned in line 9 of Algorithm 1 is the one of Equation (20). The whole procedure can be described in words as follows. First, let T_{it} denote the time limit for exploring the neighborhood of a single vertex, T_{tot} the overall time limit for the algorithm, and M the maximum number of iterations allowed. Starting from $n = 5$ and the full collection of non-isomorphic vertices of P^5_{ASEP} (See Figure 2) that we can exhaustively generate using the software Polymake [3]:

1. We apply the procedure of λ-loop break obtaining vertices of P^{n+1}_{ASEP}.
2. We complete each of these vertices with the slack variables.
3. We order all the vertices found in this way by the number of zeros, from the one with the fewest zeros to the one with the most zeros.
4. Starting from the first one, we begin to apply the Pivoting strategy as described in Section 4.1 and Equation 20. Specifically, we enumerate all possible combinations of variables that can form a feasible basis and attempt to include each of the nonbasic variables in the basis.

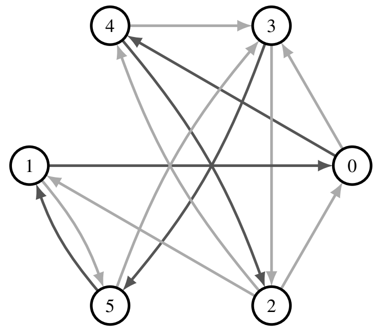

Figure 4: Starting point for the pivoting algorithm for $n = 6$.

5. When we reach the time limit T_{it}, we have a subset of adjacent vertices denoted as $\mathcal{N}'(\boldsymbol{x}) \subseteq \mathcal{N}(\boldsymbol{x})$. At this point, two things can occur:
   (a) $\mathcal{N}'(\boldsymbol{x}) = \emptyset$: In this case, we move on to the next vertex in the ordered list and start again from step 4.
   (b) $\mathcal{N}'(\boldsymbol{x}) \neq \emptyset$: in this case, we take each vertex from this set and add it to the input list, if does not belong to any of the orbits already explored, to maintain the list sorted by the number of zeros. Then, we start again from step 4.
6. We continue iteratively until either T_{tot} or M are reached.

Note that, thanks to Lemma 7, we do not need to pivot twice on isomorphic vertices, as they share the same neighborhood. In the remainder of this section, we show step-by-step how the algorithm described in Section 4 works in practice from $n = 5$ to $n = 6$. First, we need a starting vertex. To do so, we recover it using the breaking loop procedure from $n = 5$.

This gives us a representative for 6 different orbits and, among them, we choose the one with the smallest number of zeros. Figure 4 reports its support graph. Such vertex has entries equal to $\frac{k}{3}$, $k \in \{0, \dots, 5\}$. We start by pivoting from this vertex and collecting all its neighbors. Then, among its neighbors, we move to the one having the smallest number of zeros, and we proceed iteratively. Different from the pivoting pipeline presented in [13], we can recover at least one representative for each orbit.

5 Computational results

This section shows the results of our experiments, focusing on the loop-breaking procedure's impact on expanding loops and the effect on the integrality gap. Additionally, it examines the neighborhood and the stabilizer of vertices for small values of n, focusing on the relation with the integrality gap.

Implementation details All the experiments run on an ×86_64 architecture with a 13th Gen Intel(R) Core(TM) i5-13600 processor, offering 20 CPU cores with 32-bit and 64-bit operation modes. The pivoting algorithm is implemented in C++, while the iterative procedure is in Python. We use the Eigen library [18] to deal with matrices and MPFR [17] for the operations in multiple precision. The integrality gap is computed by solving the linear program (9)–(15) using Gurobi v9.5.0 [19].

5.1 Combining the symmetry breaking pivoting and the λ-loop breaking procedure

The major strength of our algorithm is that, compared to the Pivoting algorithm introduced by [13], for $n = 6$, we manage to quickly recover at least one representative for all orbits. Another strength is the impact of the λ-loop breaking procedure in quickly identifying vertices with a large integrality gap. Figure 5 illustrates this phenomenon in the transition from $n = 6$ to $n = 7$. Experimentally, we observe that the integrality gap of the vertices obtained through λ-loop breaking is always greater than or equal to the starting one. Another strength is that the λ-loop breaking procedure alone is capable of finding the vertex with the maximum integrality gap for each n. For example, in Figure 7, it can be seen that the vertex with the maximum integrality gap was obtained at iteration 0, implying that the rest of the search, although leading to many points with large integrality gaps, is subordinated to what is obtained at step 0.

Among the weaknesses, we observe that although the solutions we found with the λ-loop loops procedure are associated with large integrality gaps, they have a lot of zeros. In fact, moving from n to $n + 1$, we switch from considering

Algorithm 1: Generating vertices of P^n_{ASEP} via the explore-exploit algorithm.

Input: n, Number of nodes of the ATSP instance under study
Input: $R := \{\boldsymbol{x}_i\}_{i \in I}$, list of vertices available for $n-1$
Input: M, Maximum number of iterations of algorithm
Input: T_{tot}, time limit for the whole iterations
Input: T_{it}, timelimit for the single iteration
Output: R', a collection of non isomorphic vertices of P^n_{ASEP}

R' = Extend(R)
R' = SortByNumberOfZeros(R')
$i = 0$
$\boldsymbol{x}_0 = R'[i]$
$Ps = []$
while *$i < M$ and time $< T_{tot}$* **do**
  if *$\boldsymbol{x}_0$ is not isomorphic to any vertex in Ps* **then**
    Ps.append($\boldsymbol{x}_0$)
    $\mathcal{N}'(\boldsymbol{x_0}) =$ Pivoting($\boldsymbol{x}_0, T_{it}$)
    for $\boldsymbol{y} \in \mathcal{N}(\boldsymbol{x_0})$ **do**
      if *$\boldsymbol{y}$ is not isomorphic to any vertex in R'* **then**
        R'.insert($\boldsymbol{y}$)
      end
    end
    $i \leftarrow i + 1$
    Ps.append($R'[i]$)
  end
end
return R'

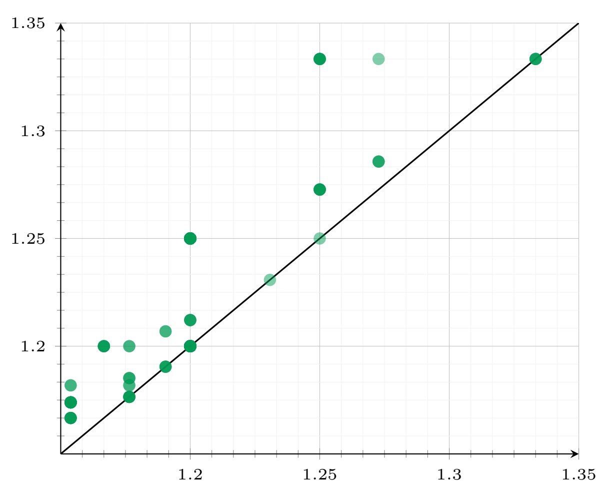

Figure 5: On the x axis, we represent the integrality gap of the vertices for $n = 6$ that have a λ-loop. For each of these vertices, we plot the integrality gap of the vertices obtained by the λ-loop breaking procedure on the y axis. The fact that all points lie (non-strictly) above the line $y = x$ implies that the λ-loop breaking procedure is highly effective in increasing the integrality gap.

points from dimension $n(n-1)$ to points in $\mathbb{R}^{(n+1)n}$, adding hence $2n$ entries. All of them are 0, but 2. So we add $2n - 2$ zeros to our vertices. Hence, it is hard to explore the full neighborhood, due to the great amount of feasible basis. Lastly, we were able to push our pivoting procedure until $n = 11$. After that, it becomes infeasible to even partially enumerate at least one neighborhood of the vertex. Figure 7 illustrates how the duration of each iteration increases and how the number of new orbits found decreases with each iteration.

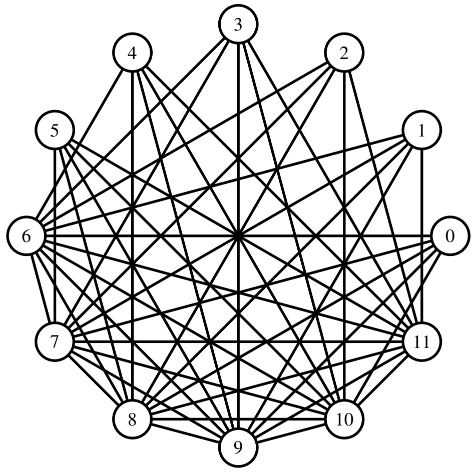

Figure 6: Polyhedral graph for P^4_{ASEP}.

Table 1: Orbit structure for $n = 4$. Columns: cardinality of the orbit, type of components, frequency of each component, and integrality gap attained at the elements of that orbit.

$\|O_{\boldsymbol{x}}\|$	Components		Frequencies		IG
6	0	1/2	4	8	$6/5$
6	0	1	8	4	1

Table 2: Orbit structure for $n = 5$. Columns: Label the orbits according to Figure 2, Cardinality of the orbit, type of components, frequency of each component, integrality gap attained at the elements of that orbit, number of tight sets, neighborhood size, and stabilizer.

	$\|O_{\boldsymbol{x}}\|$	Components			Frequencies			IG	tight sets	$\|\mathcal{N}(\boldsymbol{x})\|$	$G_{\boldsymbol{x}}$
(a)	60	0	$6/5$		10	10		$5/4$	6	28	$\langle(0\ 1)(4\ 3)\rangle$
(b)	120	0	$\frac{1}{3}$	$\frac{2}{3}$	9	7	4	$6/5$	4	20	$\langle id\rangle$
(c)	60	0	$\frac{1}{2}$		10	10		$6/5$	4	28	$\langle(0\ 4)(1\ 3)\rangle$
(d)	120	0	1	$\frac{1}{2}$	11	1	8	$6/5$	4	23	$\langle id\rangle$
(e)	24	0	1		15	5		1	10	148	$\langle(0\ 1\ 2\ 3\ 4)\rangle$

5.2 Neighborhood exploration

This section is devoted to studying the neighborhood of some vertices of $n \in \{4, 5, 6\}$ and deducing local properties. Before diving into the details, let us recall the definition of *polyhedral graph*.

Definition 8 (Polyhedral graph)**.** *A polyhedral graph is an undirected graph formed from the vertices and edges of a convex polyhedron.*

For $n = 4$, we used Polymake [3] to enumerate all the vertices of P^4_{ASEP}. This task was previously performed in [13] using PORTA [10]. More specifically, we have 12 vertices in total and two orbits. With this small number of vertices and orbits is hence easy to exhaustively study the neighborhood of each point. Figure 6 show the polyhedral graph of P^4_{ASEP}. Nodes from 0 to 5 represent the non-integer vertices, while nodes from 6 to 11 represent the tours. We can observe that each non-integer vertex has among its adjacent vertices always an integer one. Interestingly, each tour is connected to all the vertices but one.

For $n = 5$, we recover 384 vertices, as already done in [13]. We choose a representative for each class and study its neighborhood. This can be done w.l.o.g. thanks to Lemma 7. As expected, the number of neighbors is related to the degeneracy of the vertex, that is, the number of zeros among both arc and slack variables. Interestingly, each vertex has at least one adjacent representative for each equivalence class. Furthermore, the vertices (d) and (e) also have a representative of themselves among the neighbors.

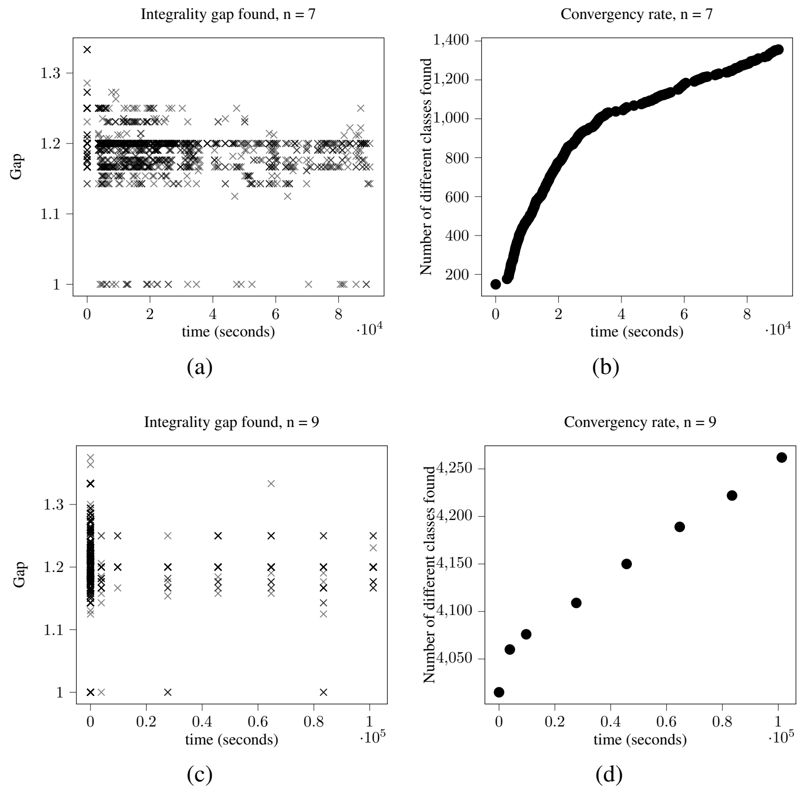

Figure 7: Left: time vs integrality gap found. The darker the $\times$, the bigger the number of vertices found leading to that integrality gap. We note that the highest integrality gap is found at the very beginning of the procedure. Right: Time vs Number of classes of isomorphism. We note that for $n = 7$ the algorithm continuously finds new and new vertices; for $n = 9$, new vertices are more and more rare.

In the case of $n = 6$, we have 90 orbits. The orbit structure can be found in Table 6 and Table 7, in the appendix. Neighborhoods of these vertices cannot be exhaustively explored. When the number of zeros is close to 18, the exhaustive listing of the whole neighborhood quickly leads to an out-of-memory error.

Note that, from our preliminary test, we state the following conjecture:

Conjecture 1. *For each $\boldsymbol{x}$ vertex, $\mathcal{N}(\boldsymbol{x})$ contains at least one tour.*

If this conjecture were true, solely pivoting on an integer vertex would lead to the full V-description of the polytope: By using Lemma 7, the neighborhood of an integer vertex will contain at least one representative of each orbit. We can then list all the vertices by fully describing each orbit. This can be done just *theoretically*, as in practice, listing the full neighborhood of a vertex with just 6 nodes is computationally infeasible.

5.3 Symmetries and conjectured relation with the integrality gap

Table 1, 2, 6, 7 show the orbit structure of $n = 4, 5, 6$. In all cases, we observe that the maximum integrality gap has been attained at a one-half integer vertex with a relatively small orbit.

Table 1 reports the structure of the orbit we found for $n = 4$. As there is only one half-integer solution, the maximum integrality gap is attained at that vertex.

For $n = 5$, we have represented all the vertices in Figure 2. The one attaining the highest integrality gap is vertex (a). Looking at Table 2, we understand that vertices (a) and (c) have the same number of non-zero and zero entries. The main differences are in the number of λ-loops and tight sets (see Definition 4). Tight sets are associated with slack variables $\overline{x}_S = 0$. In particular, vertex (a) has 6 tight sets, while vertex (c) has only 4. For $n = 6$, there are 90 orbits, see Tables 6 and 7. The vertex attaining the maximum integrality gap is again half-integer, which in principle does not seem very different from other half-integer vertices having low integrality gap (See, e.g, the middle of Table 7).

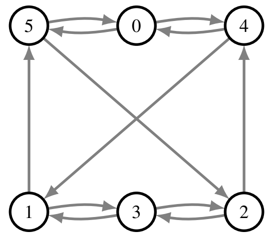

Figure 8: Vertex obtaining the maximum integrality gap for $n = 6$.

We observe that all the half-integer vertices have 10 tight sets. The two vertices having two highest integrality gaps have instead a higher number of tight sets (Lines 1 and 3 of Table 6). More specifically, the two half-integer vertices maximizing the integrality gap have, respectively, 10 and 12 tight sets.

For these small numbers of nodes, we also explicitly compute the stabilizer. For $n = 4$, the stabilizer of any representative of the non-integer orbit is given by the vertices of the subcycles in the support graph. For instance, referring to Figure 1, left, it holds $G_x = \langle (0\ 3\ 1\ 2) \rangle$.

All the stabilizers are trivial for $n = 5$, but the ones of the two half-integer vertices. Table 2 reports all the stabilizers explicitly computed. The vertices attaining the maximum gap are the ones whose stabilizer is isomorphic to $\mathbb{Z}_2$ and, more specifically, it acts by swapping the extremes of the two cycles. For vertex(c), the situation is analogous, by considering the two chained λ-loops $\overleftrightarrow{03}$ and $\overleftrightarrow{04}$ as one.

For $n = 6$, the vertex attaining the maximum integrality gap has been represented in Figure 8. The stabilizer of this vertex is isomorphic to $\mathbb{Z}_4$, more specifically it is the group generated from $(03)(1425)$. Even in this case, the stabilizer "swaps" the extreme nodes of the two chained λ-loops and the middle nodes 0 and 3.

For $n = 7$, our heuristic procedure does not recover all the vertices, hence we can do considerations only among the ones we were able to obtain, which are 1356 out of 3748. According to [13], 5 different isomorphism classes attain the maximum gap of $\frac{4}{3}$: our heuristic finds all of them. As already observed in [13], 3 out of 5 vertices have entries in $\{0, 0.5\}$ (from now on, we will denote vertices having entries in $\{0, 0.5\}$ as *half-integer*) while the others in $\{0, 0.5, 1\}$ (*integer-half-integer*). Even in this case, the number of tight sets in vertices maximizing the gap is high, namely, 12 and 16, although not maximal, as there exist pure half-integer vertices having 14 and 16 tight sets. A similar argument holds for half-integer vertices.

For $n = 8$, we identified 41 vertices with a maximum integrality gap of $\frac{4}{3}$. In [13], there were 43 of such vertices, but one of them was not half-integer. Observe that their method was specifically tailored to find *all* the half-integer vertices and *potentially* others, whereas our approach allows for more flexibility. Specifically, we discovered 17 pure half-integer orbits, 16 half-integer orbits, and 8 orbits with components in $\{0, 0.25, 0.5, 0.75\}$. While this suggests the possibility that non-half-integer vertices may also result in the maximum integrality gap, it appears to be an isolated case.

More specifically, for $n \geq 9$, the vertex attaining the maximum gap is always unique and a pure half-integer vertex. Based on our recent discussion, we have gathered the following empirical evidence:

- Among the vertices achieving the maximum integrality gap, there is at least one half-integer vertex.
- Furthermore, vertices with a large stabilizer and a large number of tight sets appear to maximize the integrality.

5.4 New lower bound on the integrality gap

Table 3 presents the results of the combined symmetry-breaking pivoting and λ-loop breaking algorithm. Starting from a vertex of P^6_{ASEP}, our combined algorithm alternates the exploration of vertices of P^n_{ASEP} with the generation of a new vertex of P^{n+1}_{ASEP}

With our combined algorithm, we can recompute all the lower bounds of α_n^{LB} up to $n = 15$, and we compute newer lower bounds for $n \in \{16, 18, 20, 22\}$ Note that for n odd, [13] introduces a family of ATSP instances having $\alpha_n = \frac{3k+1}{2k+1}$ where $n = 3 + 2(k + 1)$, which gives new lower bounds for $n = 17, 19, 21$. However, all the lower bounds in [13] are obtained only by exploring half-integer vertices, while our procedure can generate non-half-integer vertices, thanks to the λ-loop breaking procedure. However, except for the case $n = 8$, where we found a non-

Table 3: State of the art on the lower bounds $\alpha_n^{LB} \leq \alpha_n$ for ATSP, with $11 \leq n \leq 22$. In bold, the new best lower bounds are obtained with our approach. Column "n" reports the problem's dimension; Column "From [13]" provides the best-known lower bound for a given n as established in the referenced paper. Column "New" presents the lower bounds we obtained.

n	From [13]	New	n	From [13]	New
11	10/7 (1.429)	10/7 (1.429)	17	19/13 (1.461)	**55/37 (1.486)**
12	56/39 (1.436)	56/39 (1.436)	18	3/2 (1.500)	3/2 (1.500)
13	13/9 (1.444)	13/9 (1.444)	19	22/15 (1.466)	**3/2 (1.500)**
14	100/69 (1.449)	100/69 (1.449)	20	-	**3/2 (1.500)**
15	16/11 (1.454)	16/11 (1.454)	21	25/17 (1.470)	**3/2 (1.500)**
16	-	**28/19 (1.474)**	22	-	**3/2 (1.500)**

half-integer vertex maximizing the gap, such a maximum is always achieved in correspondence with a half-integer vertex.

To obtain Table 3, we proceed as follows: starting from a vertex explicitly given by [13] for $n = 18$, having an integrality gap of 1.5, we make each λ-loop *collapse* to one single node, and check time by time if the so-obtained *fesible* point is a vertex. Afterward, we expand each λ-loop, obtaining vertices for $19 \leq n \leq 22$. These two procedures built Table 3, where the best known lower bounds for the integrality gap have been reported, as well as the new ones we got with our procedure. We can observe that the lower bounds have been improved with respect to the state of the art for $n \in \{16, 17, 19, 20, 21, 22\}$. We recall that, although our exploration allows different types of fractional vertices, the maximum gap is always attained on a half-integer vertex.

5.5 Hard-ATSPLIB instances

Whenever we solve the Gap($\boldsymbol{x}$) problem to compute the maximum integrality gap for a given vertex, we generate an ATSP instance that could be challenging for ATSP solvers in practice. Hence, we propose 13 small hard ATSP instances, which we share online[1]. Several studies have examined the empirical hardness of the STSP concerning the integrality gap, such as [21, 32, 33]. However, to the best of our knowledge, no such studies have been conducted on the ATSP. Note that every time we compute the maximum possible integrality gap attained at a given vertex $\boldsymbol{x}$ by solving problem (9)–(15), we obtain a cost vector $\boldsymbol{c}$ associated to an ATSP instance having ATSP($\boldsymbol{c}$) $= 1$. Hence, we can evaluate the computational complexity of each instance as generated in this way.

A core question is how to evaluate complexity from a computational perspective. Previous work by [15] has shown promising results using a branch-and-cut algorithm that exploits facet-defining inequalities for ATSP. However, more recent studies [14, 28] suggest that Concorde, the state-of-the-art solver for the STSP, can also be a competitive method for solving ATSP instances after suitably converting them into STSP. More specifically, it is important to note that Concorde can only handle symmetric nonnegative and integer costs, but it is possible to transform any of the ATSP instances we obtained into an integer and non-negative STSP starting from the method proposed in [23]. First of all, we have observed that all the solutions we found solving Gap($\boldsymbol{x}$) are rational, and hence it is possible to make the costs integer by multiplying all the entries by the common denominator. Hence, without loss of generality, we can consider all the solutions of Gap($\boldsymbol{x}$) as integer vectors. Let $\overline{\boldsymbol{C}} = (\bar{c}_{ij})$ be a matrix derived from the cost vector as suggested in the paper of Jonker and Volgenant [23], namely:

$$\bar{c}_{ij} = \begin{cases} c_{ij} & i \neq j \\ -M & i = j, \end{cases} \tag{22}$$

where M denotes a large positive number. Consider the matrix $\boldsymbol{U}$, where all entries are set to infinity. We construct the following $\mathbb{R}^{2n \times 2n}$ matrix:

$$\tilde{\boldsymbol{C}} = \begin{bmatrix} \bar{\boldsymbol{C}} & \boldsymbol{U} \\ \boldsymbol{U} & \bar{\boldsymbol{C}} \end{bmatrix}.$$

Note that $\tilde{\boldsymbol{C}}$ may contain negative costs, which we do not want, as Concorde only performs with costs. Therefore, we shift all costs forward by M, namely making the minimum cost equal to 0. Unfortunately, in this framework, we only have *premetrics*, as we lose the triangle inequality in every triple involving two of the original nodes and one

[1] `https://github.com/eleonoravercesi/HardATSPLIB`

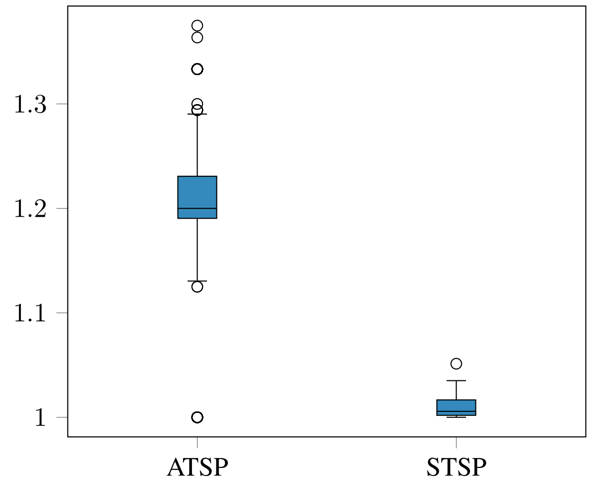

Figure 9: Distribution of the integrality gap from the ATSP to the STSP via the application of the Jonker-Volgenant-based procedure for $n = 9$.

"doubled" node. However, since we have only performed an affine translation on each cost, the optimal tour does not change. The relationship between the original values of ATSP and STSP is hence

$$\text{ATSP}(\boldsymbol{c}) = \text{STSP}(\tilde{\boldsymbol{c}}) - nM. \tag{23}$$

Hence, we transform each ATSP instance into an STSP instance as discussed above, solve each instance using Concorde, and record the computational time and the integrality gap.

Regarding the integrality gap, we observe that we only have a relation between the value of ATSP($\boldsymbol{c}$) and STSP($\tilde{\boldsymbol{c}}$), but nothing can be said *a priori* for SSEP($\tilde{\boldsymbol{c}}$) and ASEP($\boldsymbol{c}$). Remarkably, we observed that after the above-discussed procedure, the resulting instances exhibit a reduced integrality gap. Figure 9 reports this information for $n = 9$.

In terms of computational complexity, we are hence able to retrieve some hard-to-solve instances. Table 4 reports the results for the hardest instance we get for every $7 \leq n \leq 19$. We do six different types of computation:

1. We run Concorde as it is, and we record the runtime and the number of Branch & Bound (B&B) nodes. From now on, this would be called the "standard" setting, and in the Table is denoted with `-`
2. We add the flag `-d` that uses Depth-First (DF) branching instead of Breadth-First (BF). Adding this flag can prevent Concorde from writing search nodes to files, which could not be a good idea for small instances.
3. We add the flag `-C0` to disable local cuts. For small STSP instances, the computational overhead associated with generating and applying local cuts may outweigh the benefits they provide.
4. We combine the flag `-d -C0` together.
5. We run the algorithm presented in [16], here denoted with `ATSP92`, where the authors present new lower bounds for the ATSP and implement an efficient B&B exploiting them.
6. We run the algorithm presented in [14], here denoted with `FLT07`, where a Branch-and-Cut has been enhanced with the Fractionality Persistency criterion to improve the quality of the solution by prioritizing persistently fractional variables for branching.

Concorde is written in C, compiled with `gcc 13.3.0` and linked with CPLEX 12.9.0 [22]. `ATSP92` and `FLT07` are written in Fortran and compiled with `gfortran-9`. The LP in `FLT07` is solved using CPLEX 12.9.0.

For comparison, we run the same set of experiments on the instances of the ATSPLIB [27] having fewer than 100 nodes. Results can be found in Table 4 and Table 5.

First, we observe that the instances of the ATSPLIB are much easier for Concorde with respect to the ones of the HardATSPLIB. The instance `ftv38` that is twice as large as our instance with 19 nodes requires an order of magnitude less time. Overall, as expected, using DF and disabling local cuts greatly benefits the impact of Concorde. In the hardest instances, this leads to a faster runtime compared to `FLT07`. Note that, overall, Concorde is on average slower than both `ATSP95` and `FLT07`, regardless of the setting. For the hard instances, although the optimal solution is often found at the root node via primal heuristics, a large number of branching nodes are generated. Each of these nodes yields only a slight improvement in the best lower bound, which results in long runtimes to prove optimality and a lot of branching nodes. For the instances of the ATSPLIB, the lower bound is of high quality, and as such, closing the branching tree is relatively fast.

The dedicated methods `ATSP95` and `FLT07` appear more promising. `ATSP95` relies on additive bounding techniques. This makes the computation per node extremely fast. However, the absence of stronger cuts causes a rapid growth in the number of branching nodes as the instance size increases. As a result, the number of branching nodes becomes large even for relatively small instances. For instance, in `p43`, the queue size exceeds the maximum limit of 1'500'000, which prevents the solver from returning the optimal solution. However, all the instances from the HardATSPLIB are successfully solved, although the computational effort is clearly higher: for $n = 17$, the solver requires 218'251 nodes and over one second, while `br17` is solved with only 22 nodes.

`FLT07` implements a dedicated branch-and-cut algorithm specifically designed for the ATSP. It outperforms Concorde on small instances and, although slightly slower on some larger ones [14], it performs best overall on the ATSPLIB — both in terms of runtime and number of nodes. However, some interesting behavior appears when we move to the HardATSPLIB: for $n = 17, 18$, an error occurs during the root node solution phase, which prevents us from gathering complete performance data. For all other instances, the solver can prove optimality within a few seconds. Notably, the hard instance with $n = 16$ requires more than 8 seconds — nearly two orders of magnitude more than `kro124p` ($n = 100$) — and about 500 times more branching nodes.

6 Conclusions

In this paper, we have introduced and implemented a new symmetry-breaking pivoting algorithm and a new λ-loop breaking procedure that allow the exploration of vertices of the asymmetric subtour elimination polytope, yielding a large integrality gap. The symmetry-breaking pivoting exploits the class of isomorphisms of the vertices of P^n_{ASEP} that we completely calculated for a small value of n. Checking whether two vertices of P^n_{ASEP} are isomorphic is currently one of the two computational bottlenecks of our procedure. For each non-isomorphic vertex we visit, we solve an instance of the Gap($\boldsymbol{x}$) problem. With our new algorithm, we can compute new lower bounds for α_n^{LB} for $n \leq 22$ by exploring not only half-integer vertices.

As a byproduct of our generation, we propose 13 small ATSP instances that are challenging for all the solvers we tested

In the future, we plan to explore the unresolved issue addressed in this study, which involves developing a procedure that yields the stabilizer based on a vertex and creating a strategy that leverages symmetries to produce vertices that are considered *noteworthy* in terms of the integrality gap. Note that for small values of n, the integrality gap values returned by the two families of instances proposed and studied in [9, 13] are improved. For these two families, the integrality gap converges to 2. Therefore, if the improvement obtained in this paper for small values of n could be "uniformly" observed also for large values of n, this would lead to an integrality gap greater than 2. Of course, this is just an intriguing hypothesis for future research.

Another interesting research direction would be to study the integrality gap of formulations stronger than the DFJ formulation; that is, to analyze how the integrality gap evolves when additional valid inequalities, such as the Comb inequalities [11], are added. In principle, our approach can be extended to work on other polytopes, and thus it could provide insights into the worst-case instances for the integrality gap under these stronger formulations.

Acknowledgments

The work of M. Mastrolilli, L. M. Gambardella, and E. Vercesi has been supported by the Swiss National Science Foundation project n. 200021_212929/1 "Computational methods for integrality gaps analysis", Project code 36RA-GAP.

S. Gualandi acknowledges the contribution of the National Recovery and Resilience Plan, Mission 4 Component 2 - Investment 1.4 - NATIONAL CENTER FOR HPC, BIG DATA AND QUANTUM COMPUTING, spoke 6.

We thank Giovanni Rinaldi for pointing out the interesting references [26] and [4]. We are deeply indebted to Matteo Fischetti for sharing the code from [16] and [14], and for assisting us in getting it to compile and run on our machines.

Table 4: Results of the runs of different solvers on the hard instances. The first column represents the number of nodes in the ATSP instances; `(-)` indicates that Concorde was run with the default settings; `-d` refers to running Concorde with the DF option enabled; `-C0` indicates that local cuts were disabled; `-d -C0` corresponds to running Concorde with both DF enabled and local cuts disabled. `ATSP92` reports the performance from , and `FLT07` shows the performance of the algorithm presented in . The last column shows the integrality gap (`IG`) for both instances—the original ATSP and the transformed STSP, obtained through the procedure described in Section 5.5. Gaps are rounded to the third decimal place for readability.

n	-		-d		-C0		-C0 -d		ATSP92		FLT07		IG	
	Time (s)	B&B nds	Time (s)	B&B nds	Time (s)	B&B nds	Time (s)	B&B nds	Time (s)	B&B nds	Time (s)	B&B nds	STSP	ATSP
7	0.78	1	0.01	9	0.79	1	0.01	9	0.00	20	0.00	9	1.021	1.176
8	3.33	1	0.02	11	3.45	1	0.12	11	0.01	17	0.01	9	1.014	1.154
9	3.59	5	0.11	43	3.01	7	0.10	35	0.01	71	0.02	85	1.017	1.197
10	5.35	13	0.13	61	3.22	11	0.11	57	0.01	126	0.02	73	1.017	1.174
11	6.66	27	0.38	91	6.27	31	0.27	71	0.01	636	0.04	187	1.014	1.195
12	5.62	41	0.95	289	11.72	117	0.69	137	0.01	1726	0.20	939	1.014	1.212
13	25.33	217	1.18	135	14.52	165	0.83	125	0.03	5735	0.52	2271	1.015	1.248
14	22.53	285	8.99	1465	21.34	265	4.75	812	0.07	15835	2.45	9923	1.013	1.258
15	19.28	157	0.81	85	25.51	203	0.91	132	0.11	21238	0.81	2985	1.013	1.246
16	58.62	575	15.01	1461	48.38	437	3.29	385	0.41	75912	8.36	28031	1.012	1.247
17	314.79	3191	32.63	2323	90.09	1089	9.01	939	1.08	218251	-	-	1.012	1.258
18	508.98	5737	559.31	26613	515.16	5999	97.84	8701	3.16	517070	-	-	1.010	1.227
19	21.22	135	4.49	457	23.75	145	1.15	121	2.02	169364	3.62	9221	1.009	1.262

Table 5: Results of the runs of different solvers on the ATSPLIB [27]. The first two columns represent the number of nodes in the ATSP instances and the name as reported in ATSPLIB; `(-)` indicates that Concorde was run with the default settings; `-d` refers to running Concorde with the DF option enabled; `-C0` indicates that local cuts were disabled; `-d -C0` corresponds to running Concorde with both DF enabled and local cuts disabled. `ATSP92` reports the performance from , and `FLT07` shows the performance of the algorithm presented . The last column shows the integrality gap (`IG`) for both instances—the original ATSP and the transformed STSP, obtained through the procedure described in Section 5.5. Gaps are rounded to the third decimal place for readability.

Name	n	-		-d		-C0		-C0 -d		ATSP92		FLT07		IG	
		Time (s)	B&B nds	Time (s)	B&B nds	Time (s)	B&B nds	Time (s)	B&B nds	Time (s)	B&B nds	Time (s)	B&B nds	STSP	ATSP
br17	17	0.01	1	0.01	1	0.01	1	0.01	1	0.01	22	0.00	1	1.000	1.000
ftv33	34	0.01	1	0.02	1	0.01	1	0.01	1	0.01	164	0.00	1	1.000	1.010
ftv35	36	0.34	5	0.08	11	0.38	5	0.06	9	0.03	1108	0.01	11	1.001	1.011
ftv38	39	0.99	5	0.11	11	1.32	9	0.12	11	0.04	1403	0.02	17	1.001	1.010
p43	43	2.04	17	0.39	33	0.75	11	0.22	31	25.32*	174562*	0.34	277	1.000	1.002
ftv44	45	0.35	3	0.22	15	0.45	5	0.23	19	0.02	340	0.04	35	1.001	1.018
ry48p	48	1.41	3	0.24	15	1.75	5	0.24	17	2.24	25910	0.14	89	1.000	1.016
ftv47	48	0.43	5	0.22	9	0.49	5	0.20	11	0.14	5495	0.13	165	1.001	1.016
ft53	53	0.03	1	0.02	1	0.02	1	0.03	1	0.02	141	0.01	1	1.000	1.000
ftv55	56	1.06	5	0.18	5	1.00	5	0.18	5	0.21	9245	0.08	107	1.001	1.015
ftv64	65	1.19	5	0.15	15	1.78	7	0.17	17	0.41	8224	0.12	119	1.001	1.018
ft70	70	0.29	3	0.10	7	0.29	1	0.10	7	0.03	276	0.01	7	1.000	1.001
ftv70	71	1.05	7	0.20	21	1.25	5	0.21	21	1.29	21606	0.35	277	1.001	1.021
kro124p	100	0.32	1	0.58	17	0.30	1	0.58	23	6.33	17387	0.18	59	1.000	1.009

A Detailed description of the orbits for for $n = 6$

Table 6: Orbit structure for $n = 6$, top 21 having the highest integrality gap. Columns: cardinality of the orbit, type of components, frequency of each component, and integrality gap attained at the elements of that orbit.

$\lvert O_{\boldsymbol{x}} \rvert$	Components				Frequencies				IG
180	0	1/2			18	12			4/3
120	0	1/3	2/3		18	6	6		9/7
360	0	1/2			18	12			14/11
360	0	1/2			18	12			5/4
720	0	1/2			18	12			5/4
180	0	1/2			18	12			5/4
720	0	1	1/2		19	1	10		5/4
720	0	1	1/2		19	1	10		5/4
360	0	1	1/2		19	1	10		5/4
720	0	1/4	3/4	1/2	17	5	3	5	16/13
720	0	1/4	3/4	1/2	16	6	2	6	6/5
720	0	1/4	3/4	1/2	16	6	2	6	6/5
720	0	1/4	3/4	1/2	17	5	3	5	6/5
720	0	1/4	3/4	1/2	16	6	2	6	6/5
720	0	1/4	3/4	1/2	16	6	2	6	6/5
720	0	1/4	3/4	1/2	16	6	2	6	6/5
720	0	1/4	3/4	1/2	16	6	2	6	6/5
720	0	1/4	3/4	1/2	16	6	2	6	6/5
720	0	1/4	3/4	1/2	16	6	2	6	6/5
720	0	1/4	3/4	1/2	16	6	2	6	6/5
720	0	1/4	3/4	1/2	17	5	3	5	6/5

Table 7: Orbit structure for $n = 6$, bottom 69 having the lowest integrality gap. Columns: cardinality of the orbit, type of components, frequency of each component, and integrality gap attained at the elements of that orbit.

$\lvert O_{\boldsymbol{x}} \rvert$	Components					Frequencies					IG
720	0	$1/3$	$2/3$			17	8	5			$6/5$
720	0	$1/3$	$2/3$			16	10	4			$6/5$
720	0	$1/3$	$2/3$			16	10	4			$6/5$
720	0	$1/3$	$2/3$			16	10	4			$6/5$
720	0	$1/3$	$2/3$			16	10	4			$6/5$
720	0	$1/3$	$2/3$			16	10	4			$6/5$
720	0	$1/3$	$2/3$			16	10	4			$6/5$
720	0	$1/3$	$2/3$			16	10	4			$6/5$
720	0	$1/3$	$2/3$			16	10	4			$6/5$
720	0	$1/3$	$2/3$			16	10	4			$6/5$
720	0	$1/3$	$2/3$			16	10	4			$6/5$
720	0	$1/3$	$2/3$			17	8	5			$6/5$
720	0	$1/3$	$2/3$			17	8	5			$6/5$
720	0	$1/3$	$2/3$			17	8	5			$6/5$
720	0	$1/3$	$2/3$			17	8	5			$6/5$
720	0	$1/3$	$2/3$			17	8	5			$6/5$
720	0	$1/3$	$2/3$			17	8	5			$6/5$
720	0	$1/3$	$2/3$			16	10	4			$6/5$
720	0	$1/3$	$2/3$			17	8	5			$6/5$
720	0	$1/3$	$2/3$			17	8	5			$6/5$
720	0	$1/3$	$2/3$			17	8	5			$6/5$
720	0	$1/3$	$2/3$			17	8	5			$6/5$
720	0	$1/3$	$2/3$			16	10	4			$6/5$
720	0	$1/3$	$2/3$			17	8	5			$6/5$
720	0	$1/3$	$2/3$			17	8	5			$6/5$
240	0	$1/3$	$2/3$			18	6	6			$6/5$
720	0	$1/3$	$2/3$			16	10	4			$6/5$
720	0	$1/3$	$2/3$			17	8	5			$6/5$
720	0	$1/3$	$2/3$			17	8	5			$6/5$
720	0	$1/3$	$2/3$			16	10	4			$6/5$
120	0	$1/2$				18	12				$6/5$
720	0	$1/2$				18	12				$6/5$
720	0	$1/2$				18	12				$6/5$
720	0	$1/2$				18	12				$6/5$
720	0	$1/2$				18	12				$6/5$
720	0	1	$1/3$	$2/3$		18	1	7	4		$6/5$
720	0	1	$1/3$	$2/3$		18	1	7	4		$6/5$
720	0	1	$1/3$	$2/3$		18	1	7	4		$6/5$
720	0	1	$1/3$	$2/3$		18	1	7	4		$6/5$
360	0	1	$1/2$			19	1	10			$6/5$
720	0	1	$1/2$			19	1	10			$6/5$
720	0	1	$1/2$			19	1	10			$6/5$
720	0	1	$1/3$	$2/3$		18	1	7	4		$6/5$
360	0	1	$1/2$			20	2	8			$6/5$
720	0	1	$1/2$			20	2	8			$6/5$
720	0	1	$1/2$			20	2	8			$6/5$
720	0	$1/5$	$4/5$	$2/5$	$3/5$	16	5	2	4	3	$25/21$
720	0	$1/5$	$4/5$	$2/5$	$3/5$	16	5	2	4	3	$25/21$
720	0	$1/5$	$4/5$	$2/5$	$3/5$	16	5	2	4	3	$25/21$
720	0	$1/4$	$3/4$	$1/2$		16	7	3	4		$20/17$
720	0	$1/4$	$3/4$	$1/2$		16	7	3	4		$20/17$
720	0	$1/4$	$3/4$	$1/2$		16	7	3	4		$20/17$
720	0	$1/4$	$3/4$	$1/2$		16	7	3	4		$20/17$
720	0	$1/4$	$3/4$	$1/2$		16	7	3	4		$20/17$
720	0	$1/4$	$3/4$			16	9	5			$20/17$
720	0	$1/3$	$2/3$			16	10	4			$7/6$
120	0	$1/2$				18	12				$7/6$
720	0	$1/3$	$2/3$			16	10	4			$15/13$
720	0	$1/3$	$2/3$			17	8	5			$15/13$
360	0	$1/3$	$2/3$			16	10	4			$15/13$
720	0	$1/3$	$2/3$			16	10	4			$15/13$
720	0	$1/3$	$2/3$			16	10	4			$15/13$
720	0	$1/3$	$2/3$			16	10	4			$15/13$
720	0	$1/3$	$2/3$			16	10	4			$15/13$
360	0	$1/3$	$2/3$			16	10	4			$15/13$
720	0	$1/3$	$2/3$			17	8	5			$15/13$
720	0	$1/3$	$2/3$			17	8	5			$15/13$
120	0	$1/3$	$2/3$			18	6	6			$15/13$
120	0	1				24	6				1

References

[1] David Applegate et al. "On the solution of traveling salesman problems." eng. In: *Documenta Mathematica* (1998), pp. 645–656. URL: `http://eudml.org/doc/233207`.

[2] Michael Artin. *Algebra*. Upper Saddle River, NJ: Pearson Education, 2011.

[3] Benjamin Assarf et al. "Computing convex hulls and counting integer points with polymake". In: *Math. Program. Comput.* 9.1 (2017), pp. 1–38.

[4] M. L. Balinski and Andrew Russakoff. "On the Assignment Polytope". In: *SIAM Review* 16.4 (1974), pp. 516–525. DOI: 10.1137/1016083. eprint: https://doi.org/10.1137/1016083. URL: https://doi.org/10.1137/1016083.

[5] Genevieve Benoit and Sylvia Boyd. "Finding the exact integrality gap for small Traveling Salesman Problems". In: *Mathematics of Operations Research* 33.4 (2008), pp. 921–931.

[6] Sylvia Boyd et al. "TSP on cubic and subcubic graphs". In: *Integer Programming and Combinatoral Optimization: 15th International Conference, IPCO 2011, New York, NY, USA, June 15-17, 2011. Proceedings 15*. Springer. 2011, pp. 65–77.

[7] Sylvia C. Boyd and Paul Elliott-Magwood. "Computing the integrality gap of the asymmetric travelling salesman problem". In: *Electron. Notes Discret. Math.* 19 (2005), pp. 241–247.

[8] Robert Carr and Santosh Vempala. "On the Held-Karp relaxation for the Asymmetric and Symmetric Traveling Salesman Problems". In: *Mathematical Programming* 100.3 (2004), pp. 569–587.

[9] Moses Charikar, Michel X Goemans, and Howard Karloff. "On the integrality ratio for the Asymmetric Traveling Salesman Problem". In: *Mathematics of Operations Research* 31.2 (2006), pp. 245–252.

[10] Thomas Christof. "Porta". In: *http://www.iwr.uni-heidelberg. de/groups/comopt/software/PORTA/index. html* (2009).

[11] Václav Chvátal. "Edmonds polytopes and weakly Hamiltonian graphs". In: *Mathematical programming* 5 (1973), pp. 29–40.

[12] George Dantzig, Ray Fulkerson, and Selmer Johnson. "Solution of a large-scale traveling-salesman problem". In: *Journal of the operations research society of America* 2.4 (1954), pp. 393–410.

[13] Paul Elliott-Magwood. "The integrality gap of the Asymmetric Travelling Salesman Problem". PhD thesis. University of Ottawa (Canada), 2008.

[14] Matteo Fischetti, Andrea Lodi, and Paolo Toth. "Exact methods for the Asymmetric Traveling Salesman Problem". In: *The traveling salesman problem and its variations* (2007), pp. 169–205.

[15] Matteo Fischetti and Paolo Toth. "A polyhedral approach to the Asymmetric Traveling Salesman Problem". In: *Management Science* 43.11 (1997), pp. 1520–1536.

[16] Matteo Fischetti and Paolo Toth. "An additive bounding procedure for the asymmetric travelling salesman problem". In: *Mathematical programming* 53 (1992), pp. 173–197.

[17] Laurent Fousse et al. "MPFR: A multiple-precision binary floating-point library with correct rounding". In: *ACM Transactions on Mathematical Software (TOMS)* 33.2 (2007), 13–es.

[18] Gaël Guennebaud and Benoît Jacob. *Eigen v3*. http://eigen.tuxfamily.org. 2010.

[19] Gurobi Optimization, LLC. *Gurobi Optimizer Reference Manual*. 2023. URL: https://www.gurobi.com.

[20] Stefan Hougardy. "On the integrality ratio of the subtour LP for Euclidean TSP". In: *Operations Research Letters* 42.8 (2014), pp. 495–499. ISSN: 0167-6377.

[21] Stefan Hougardy and Xianghui Zhong. "Hard to solve instances of the Euclidean Traveling Salesman Problem". In: *Mathematical Programming Computation* 13 (2021), pp. 51–74.

[22] IBM Corporation. *IBM ILOG CPLEX Optimization Studio*. Version 12.9.0. 2019. URL: https://www.ibm.com/products/ilog-cplex-optimization-studio.

[23] Roy Jonker and Ton Volgenant. "Transforming Asymmetric into Symmetric Traveling Salesman Problems". In: *Operations Research Letters* 2.4 (1983), pp. 161–163.

[24] F. William Lawvere. "Metric spaces, generalized logic, and closed categories". In: *Rendiconti del Seminario Matematico e Fisico di Milano* 43.1 (Dec. 1973), pp. 135–166.

[25] Matthias Mnich and Tobias Mömke. "Improved integrality gap upper bounds for traveling salesperson problems with distances one and two". In: *European journal of operational research* 266.2 (2018), pp. 436–457.

[26] M.W. Padberg and M.R. Rao. "The Travelling Salesman Problem and a Class of Polyhedra of Diameter Two". In: *Mathematical Programming* 7 (1974), pp. 32–45.

[27] Gerhard Reinelt. "TSPLIB—A traveling salesman problem library". In: *ORSA journal on computing* 3.4 (1991), pp. 376–384.

[28] Roberto Roberti and Paolo Toth. "Models and algorithms for the Asymmetric Traveling Salesman Problem: an experimental comparison". In: *EURO Journal on Transportation and Logistics* 1.1-2 (2012), pp. 113–133.

[29] Mohit Singh. "Integrality gap of the vertex cover linear programming relaxation". In: *Operations Research Letters* 47.4 (2019), pp. 288–290.

[30] Vera Traub and Jens Vygen. "An improved approximation algorithm for ATSP". In: *Proceedings of the 52nd annual ACM SIGACT symposium on theory of computing*. 2020, pp. 1–13.

[31] Vijay V. Vazirani. *Approximation Algorithms*. Vol. 1. Berlin: Springer, 2001.

[32] Eleonora Vercesi et al. “On the generation of metric TSP instances with a large integrality gap by branch-and-cut”. In: *Mathematical Programming Computation* 15.2 (2023), pp. 389–416.

[33] Xianghui Zhong. “Lower bounds on the integrality ratio of the subtour LP for the traveling salesman problem”. In: *Discrete Applied Mathematics* 365 (2025), pp. 109–129. ISSN: 0166-218X.